Available online at www.sciencedirect.com
ScienceDirect
Journal of Nuclear Materials 372 (2008) 66–75
journal of nuclear materials
www.elsevier.com/locate/jnucmat

The effect of phosphorus on creep in copper

Rolf Sandström [a,b,*], Henrik C.M. Andersson [b]

[a] Materials Science and Engineering, Royal Institute of Technology, Brinellvägen 23, S-10044 Stockholm, Sweden
[b] Corrosion and Metals Research Institute, Drottning Kristinas väg 48, S-11428 Stockholm, Sweden

Received 30 January 2007; accepted 23 February 2007

Abstract

Pure copper with an addition of about 50 ppm phosphorus is the planned material for the outer part of the waste package for spent nuclear fuel in Sweden. Phosphorus is added to improve the creep ductility but it also strongly increases the creep strength. In the present paper the influence of phosphorus on the strength properties of copper is analysed. Using the Labusch–Nabarro model it is demonstrated that 50 ppm has a negligible influence on the yield strength in accordance with observations. For slow moving dislocations, the interaction energy between the P-atoms and the dislocations gives rise to an agglomeration and a locking. The computed break away stresses are in agreement with the difference in creep stress of copper with and without P-additions.

PACS: 83.10.Gr; 81.70.Bt; 87.15.La

1. Background

It has been known for a long time that phosphorus enhances the creep strength of pure copper. Although their studies were limited to the initial stages of primary creep, Burghoff and Blank clearly demonstrated that the deoxidation of pure copper with 80 ppm P reduced the creep rates [1,2]. Again primary creep was the main interest of Kouta and Webster [3]. Their main finding was that both primary and secondary creep can be described by a single expression. The first who generated design data for P-deoxidised Cu based on long term creep tests were Drehfahl et al. [4]. They performed tests up to 20 000 h. The P-content of their alloys was 200 ppm. They showed that P-deoxidised Cu has an adequate creep ductility and that the material is suitable for pressure vessels.

Andersson et al. studied the influence of phosphorus on the creep properties of oxygen free copper [5]. It was demonstrated that the creep strength and creep ductility were improved at 175 °C when 30 ppm P was added. No significant further improvement was observed when the P-content was raised more. The room temperature tensile properties were not noticeably influenced by the P-content. The phosphorus is in solid solution. Pure copper can dissolve up to 3.5 wt% P [6].

Hutchinson and Ray found that phosphorus, at least in larger concentrations, has a pronounced effect on both recovery and recrystallization [7]. They studied copper with 0.16 and 0.76 wt% P. When annealing 95% cold rolled sheet they observed that both processes could be retarded by more than a factor 1000. The influence on the recovery rate has a direct relevance for the creep behaviour since recovery of dislocations is often rate controlling. Hutchinson and Ray attributed the recovery retardation to the impurity locking of the dislocations. Further evidence for this conclusion was the fact that they observed strain ageing, which is in general believed to be caused by the locking of dislocations, see, e.g. [8]. It is the purpose of this paper

* Corresponding author. Address: Materials Science and Engineering, Royal Institute of Technology, Brinellvägen 23, S-10044, Stockholm, Sweden. Fax: +46 8 203107.
E-mail address: rsand@kth.se (R. Sandström).

0022-3115/$ - see front matter © 2007 Elsevier B.V. All rights reserved.
doi:10.1016/j.jnucmat.2007.02.004

to present models for the influence of P-solutes on the strength properties of copper.

2. Models for the influence of solutes

2.1. Labusch–Nabarro model

According to the Labusch–Nabarro model [9,10], the increase in the yield strength $\Delta R_{p0.2}$ is [11]

$$\Delta R_{p0.2} = K_{LN} \cdot \varepsilon_b^{4/3} \cdot c^{2/3}, \tag{1}$$

where K_{LN} is a constant. ε_b is the lattice misfit parameter which is 0.1651 for P in Cu [12]. c is the atomic fraction of the solutes. The model value for K_{LN} in MPa is

$$K_{LN} = 1.1 \times 10^{-3} \frac{m\alpha^{4/3} w^{1/3} G}{b^{1/3}}, \tag{2}$$

where m is the Taylor factor for fcc (3.06), $\alpha = 16$ is a constant. The interaction distance between solute and dislocation w is set to 2–5b, where b is Burgers vector and G the shear modulus. These assumptions give K_{LN} the value of 10400 MPa and $\Delta R_{p0.2} = 0.6$–0.8 MPa, which is a very small increase in the yield strength. This is also consistent with measured properties for pure copper with and without phosphorus. Handbook data gives no difference in tensile properties [13].

2.2. Solid solution during creep

The velocity v_{climb} of a climbing dislocation in a metal during creep can be expressed as [14]

$$v_{climb} = M_{climb} b \sigma_{app}, \tag{3}$$

where σ_{app} is the applied stress and M_{climb} the climb mobility

$$M_{climb} = \frac{D_s b}{kT}, \tag{4}$$

where D_s is the self diffusion coefficient, k is the Boltzmann constant and T the absolute temperature. The time t_0 for a dislocation to move one atomic distance is then given by

$$t_0 = \frac{b}{v_{climb}}. \tag{5}$$

Stresses from the solutes retard the dislocation. This can be taken into account by introducing the interaction energy E between the solute and the dislocation. In the elastic approximation the maximum value of E is given by [14]

$$E = -\frac{1}{2\pi} \frac{(1+v)}{(1-v)} G v_a \varepsilon_b, \tag{6}$$

where v is Poisson's number and v_a the atomic volume. Inserting values for Cu gives -2.5×10^{-20} J at room temperature. The average time for the dislocation to pass a solute can be expressed as

$$t_{eff} = t_0 e^{\frac{|E|}{kT}}. \tag{7}$$

In addition the solute must diffuse away from the front of the dislocation. Using Einstein's equation the time t_{diff} can be expressed as

$$t_{diff} = \frac{b^2}{2D_P}, \tag{8}$$

where D_P is the diffusion coefficient for the P-solute in Cu. The total time for the dislocation to pass the solute is then $t_{tot} = t_{eff} + t_{diff}$. The relative increase in time t_{tot}/t_0 takes the form

$$\frac{t_{tot}}{t_0} = e^{\frac{|E|}{kT}} + \frac{b^3 D_s \sigma_{app}}{2 D_P kT}. \tag{9}$$

Since $b^3\sigma_{app}/2kT < 1$ for Cu and $D_P \gg D_s$ for P in Cu, see Section 2.3, the second term is negligibly small. Eq. (9) gives $t_{tot}/t_0 = 179$, 93, and 56 at 75, 125 and 175 °C, respectively. If the corresponding analysis would be performed for glide instead, the only difference would be that the second term in Eq. (9) would disappear. Thus the result would be numerically identical since this term is negligible.

2.3. Solute drag

If solutes are attracted to the dislocations a Cottrell atmosphere might be formed, which creates a drag force. The interaction energy between a solute atom and an edge dislocation can be expressed as

$$W = -\frac{2bE}{3} \frac{y}{x^2 + y^2}, \tag{10}$$

where (x, y) is the position of the solute relative to a dislocation that is climbing in the y-direction or gliding in the x-direction, see Fig. 1.

The variation of the interaction energy according to Eq. (10) is illustrated in Fig. 2. For a climbing dislocation the solutes are repelled above the dislocation ($y > 0$) and attracted to the dislocation below ($y < 0$). For a gliding dislocation the P-solutes will primarily be positioned below the edge dislocation ($y < 0$), because the solutes are larger than the parent atoms and the interaction energy is

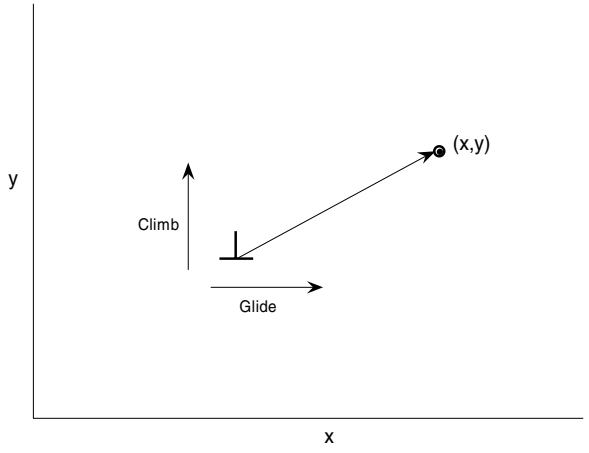

Fig. 1. Coordinate system for a climbing or gliding edge dislocation.

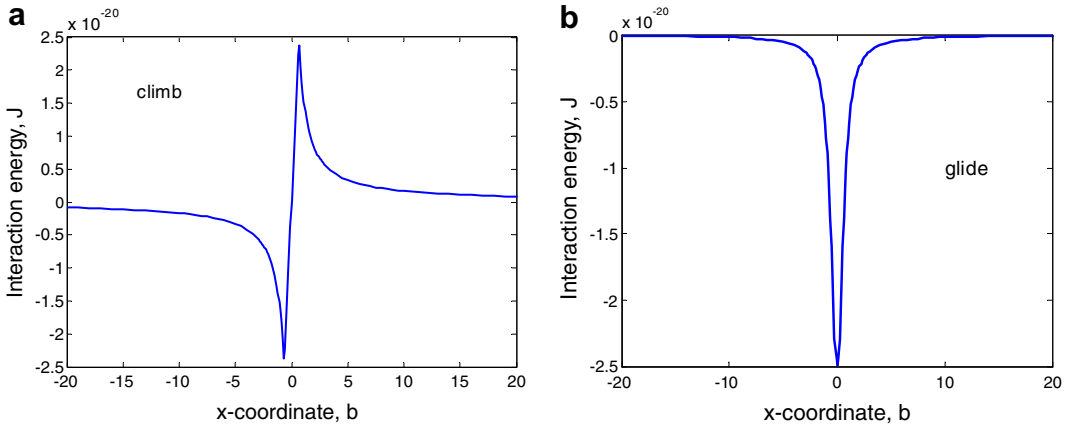

Fig. 2. Interaction energy between a dislocation and a P-atom taken at the core radius: (a) climb and (b) glide.

negative. The values in Fig. 2 are shown at the core radius, which is chosen as $2/3b$. The reason for the selection of this core radius is that it gives a maximum interaction energy E that is in reasonable agreement with observed values for the binding energy [15].

For a static (not moving) dislocation the concentration of solutes around a dislocation c_{Pstat} is given by [14]

$$c_{\mathrm{Pstat}} = c_{\mathrm{P0}} \mathrm{e}^{-\frac{W}{kT}}. \tag{11}$$

This expression is illustrated in Figs. 3 and 4 for a climbing and a gliding dislocation, respectively.

For climb there is a trough in the solute concentration in front of the dislocation and a peak behind it, see Fig. 3. Below a gliding dislocation on the other hand there is a pronounced concentration of solutes, see Fig. 4.

For a dislocation moving with a Cottrell atmosphere of solutes, the diffusion equation can be solved. Hirth and Lothe gave the following solution [14]:

$$c_{\mathrm{Pdyn}} = \frac{v c_{\mathrm{P0}}}{D_{\mathrm{P}}} \left(\mathrm{e}^{-\frac{W(y)}{kT} - \frac{vy}{D_{\mathrm{P}}}} \right) \int_{-\infty}^{y} \mathrm{e}^{\frac{W(y')}{kT} + \frac{vy'}{D_{\mathrm{P}}}} \mathrm{d}y', \tag{12}$$

where v is the velocity of the dislocation. Using the interaction energy in Eq. (10) and climb velocity in Eq. (3) with an applied stress of 150 MPa, the values for c_{Pdyn} have been computed, see Fig. 3. The difference in comparison with the static solution is that both the peak and the trough around the dislocation are much more pronounced. The height of the peak is increased with decreasing temperature.

For a gliding dislocation, Eq. (12) can again be used but with a different interaction energy and integrated along the x-axis instead. The result is illustrated in Fig. 4. A dislocation glide velocity corresponding to a strain rate of $1 \times 10^{-8}\ \mathrm{s}^{-1}$ has been used. The glide and the climb velocities are then about the same at 175 °C. Also in the glide case the peak around the dislocation is higher in the dynamic case than in the static one. A small trough in front of the dislocation is observed at the lowest temperature 75 °C.

From the distribution of the solutes, the excess solute concentration around the peak at the dislocation can be determined

$$c_{\mathrm{Pexc}} = \int_{y_{\mathrm{L}}}^{y_{\mathrm{R}}} (c_{\mathrm{Pdyn}} - c_{\mathrm{P0}}) \mathrm{d}y. \tag{13}$$

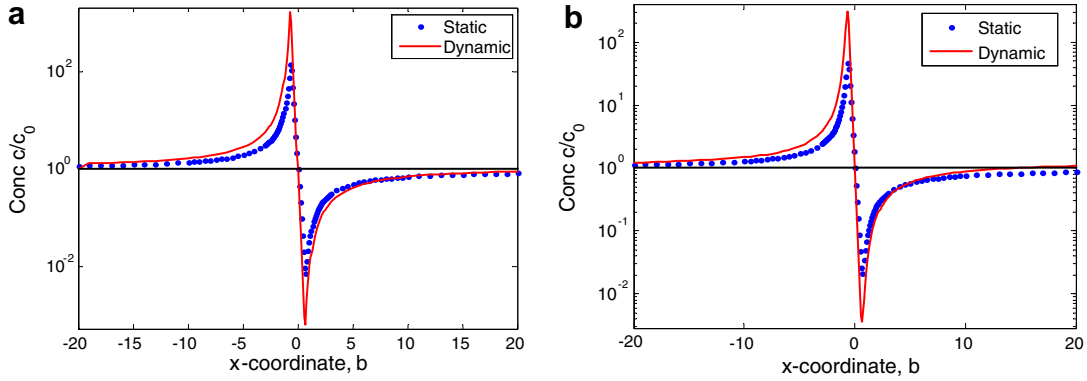

Fig. 3. Concentration c/c_0 of P-atoms relative to the equilibrium value as a function of distance from a climbing dislocation moving in the positive y-direction. Static, non-moving dislocation. Dynamic, moving dislocation. (a) 75 °C and (b) 175 °C.

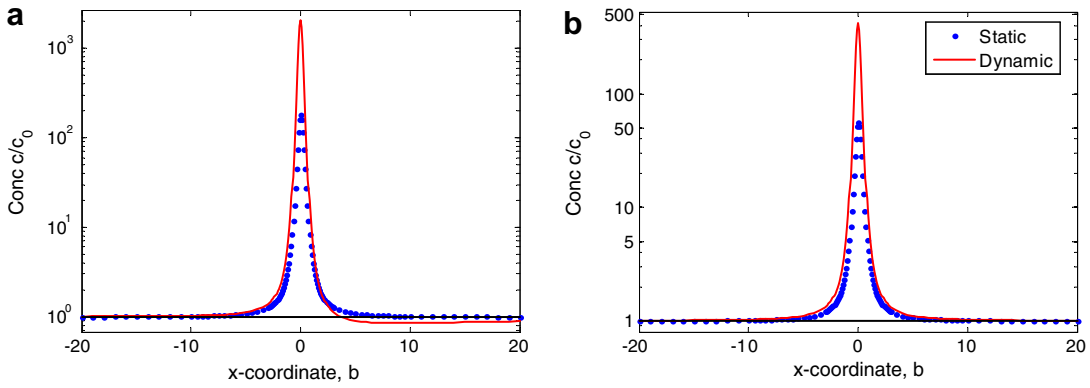

Fig. 4. Concentration c/c_0 of P-atoms relative to the equilibrium value as a function of distance from a gliding dislocation moving in the positive x-direction. Static, non-moving dislocation. Dynamic, moving dislocation. (a) 75 °C and (b) 175 °C.

Table 1
Values assessed from the profiles in Figs. 3 and 4

	75 °C	125 °C	175 °C
Climb			
$c_{\mathrm{Pexc}}/c_{\mathrm{P0}}$	506	226	122
σ_{y} (MPa)	0.012	0.007	0.008
$\sigma_{\mathrm{ydrag}\infty}$ (MPa)	0.005	0.008	0.012
Glide			
$c_{\mathrm{Pexc}}/c_{\mathrm{P0}}$, $\dot{\varepsilon} = 1\mathrm{e}^{-8}\ \mathrm{s}^{-1}$	998	474	243
σ_{x} (MPa)	0.99	0.03	0.001
$\sigma_{\mathrm{xdrag}\infty}$ (MPa)	1.5	0.04	0.002

For climb $y_{\mathrm{L}} = -5b$ and $y_{\mathrm{R}} = 0$ are chosen. For glide the integration is performed in the x-direction with $x_{\mathrm{L}} = -5b$ and $x_{\mathrm{R}} = 5b$. The results are given in Table 1.

From Table 1 it is evident that the increase in solute concentration at the dislocation is quite high and can reach values of 1000. For glide the enhancement is about twice that for climb. The solute enrichment increases with decreasing temperature.

The presence of the solutes creates a drag stress σ_{drag} that retards the dislocations

$$\sigma_{\mathrm{drag}} = \int_{y_{\mathrm{L}}}^{y_{\mathrm{R}}} c_{\mathrm{Pdyn}} \left(-\frac{\partial W}{\partial y} \right) \mathrm{d}y. \tag{14}$$

In this case as well, the integration range is taken as $\pm 5b$ for a gliding dislocation. Nominally the range could be much larger but it is believed that the effect of solutes further away is screened off. The integration range does not have a pronounced effect on the result. The computed drag stresses are shown in Table 1. As can be seen they are always very small, partially due to the fairly rapid diffusion of P-atoms. For climb the drag forces are even smaller than for glide.

There is also another way to estimate the drag force [14,16]. The derivation is similar to that of Eq. (13)

$$\sigma_{\mathrm{drag}\infty} = \frac{kTv}{b^2 D_{\mathrm{P}}} N_{\mathrm{Pexc}}, \tag{15}$$

where v is the climb or glide velocity, and the excess number of solutes is

$$N_{\mathrm{Pexc}} = \int_{-\infty}^{\infty} (c_{\mathrm{Pdyn}} - c_{\mathrm{P0}}) \mathrm{d}y. \tag{16}$$

One difference between Eqs. (14) and (15) is that in the former case only the effective range close to the dislocation is taken into account. Another one is that the approximations in deriving the expressions are different [14]. Results for $\sigma_{\mathrm{drag}\infty}$ are given in Table 1. The two sets of values for the drag stress are of the same order of magnitude.

2.4. Break away of looked dislocations

In Sections 2.1 and 2.3 different ways of handling solid solution hardening have been presented. Both methods suggest a very small effect of the order of 1 MPa or less. Experimentally for slow high temperature deformation there is a very large effect of the P-atoms in solid solution. The reason for this discrepancy is that the effect cannot be fully described by a continuous diffusion equation. The solutes must break away from the dislocation to enable it to move. The additional stress σ_{break} that is needed can be computed from the energy that is required to move a dislocation one Burgers vector. According to Peach–Koehler's formula the force on the dislocation segment of length $2L$ is $F = \sigma_{\mathrm{break}} 2Lb$. The consumed energy is then $Fb/2$. An energy balance gives

$$\sigma_{\mathrm{break}} L b^2 = E(1 - \sigma_{\mathrm{app}}/\sigma_{\mathrm{m}}). \tag{17}$$

The factor in the brackets takes into account that the break stress must vanish when the tensile strength σ_{m} is reached. The average distance L between the solutes that pin the dislocation is

$$L = \frac{b}{c_{\mathrm{Pexc}} + c_{\mathrm{P0}}}, \tag{18}$$

where the excess concentration at the dislocation is given in atom fraction. Combining Eqs. (13), (17) and (18) gives

$$\sigma_{\text{break}} = \frac{E}{b^3}(1-\sigma_{\text{app}}/\sigma_{\text{m}})\int_{y_{\text{L}}}^{y_{\text{R}}} c_{\text{Pdyn}}\,\mathrm{d}y, \tag{19}$$

where c_{Pdyn} is given by Eq. (12).

3. Analysis of creep data

3.1. Data on the influence of phosphorus on creep in copper

The composition and mechanical properties of the batches of oxygen free copper Cu-OF and of oxygen free copper with phosphorus Cu-OFP that will be used to analyse the role of phosphorus are listed in Table 2.

The first four batches are made of pure Cu-OF whereas the remainder are phosphorus alloyed. All the batches except the final one, 900, have been creep strain tested. For 900 slow strain tensile testing has been used. In spite of the fact that this batch has been cold worked, this influences the stationary stress only marginally. The slow strain rate tests are valuable since they provide stationary stresses even at low temperatures for Cu-OFP (Table 3).

3.2. Diffusion constants

In the modelling diffusion constants are needed. The used constants are summarised in Table 4. For bulk diffusion, the self diffusion coefficient has been taken from Neumann et al. [21]. Similar values for the coefficient have been obtained in ab initio calculations [22]. For grain boundary diffusion the values from [23] have been used. Other values for high purity copper can be found in [24,25]. They are associated with activation energies that are even lower than for pipe diffusion, which has not been considered as realistic for normal purity copper.

Pipe diffusion coefficients have been computed from the bulk diffusion values applying the principles in [26,27]. For P in copper, bulk diffusion coefficients are available in Landolt-Börnstein [28]. Experimental values for grain boundary or pipe diffusion have not been found. For pipe diffusion the principles in [26,27] have again been used. For grain boundary diffusion the activation energy has been scaled to that for bulk self diffusion and the pre-exponential factor has been kept unchanged.

3.3. Representation of the creep data

The stress dependence of the minimum creep rate is quite different for Cu-OF and Cu-OFP. This has the consequence that a direct comparison of their creep data is not possible. Instead the data has to be represented by models. Suitable models have been set up in [29].

The minimum creep rate $\dot{\varepsilon}_{\text{crmin}}$ is represented by the following expression:

$$\left.\frac{\mathrm{d}\varepsilon_{\text{cr}}}{\mathrm{d}t}\right|_{\text{min}} = A\sigma^{n(T)}\mathrm{e}^{\beta(\sigma)}\mathrm{e}^{-\frac{q(T)}{RT}}. \tag{20}$$

Table 2
Characteristics of analysed materials

Material number	Other batch id	Grain size (μm)	P (ppm)	S (ppm)	H (ppm)	O (ppm)	Yield strength $R_{\text{p0.2}}$ (MPa)	Tensile strength R_{m} (MPa)	Elongation (%)	Reduction in area Z (%)	Hardness (HV)
000	Cu_OF000	60	2	10	0.16	1.20					
100	Cu_OF100	370	2	10	0.69	1.60					
200	Cu_OF200	45	<1	6	<0.10	1.10	50	234	61		42
1	CuP0_300	300	<1	6	<0.5	1.1	62	228	45		55
2	CuP30_450	450	29	6	<0.5	1.2					53
3	CuP60_350	350	58	6	<0.5	1.1	52	225	45		55
4	CuP105_450	450	106	5	<0.5	1.1	51	224	46		–
6	CuP60_100	100	58	6	<0.5	–	56	231	46		55
400[a]	Cu-OFP400	45	50	6	<0.10	0.90	46	239	60		40
400[a]	Cu-OFP400		59				97	243	46	94	54
500	Cu-OFP500		54				93	202	42	76	53
900	Cu-OFP SSR		50[b]				209	226			116

[a] Two assessments have been performed.
[b] Specified value.

Table 3
Creep and slow strain rate tests included in the assessment

Material number	Other batch id	Test temperatures and number of specimens (°C)	Comment	Reference
000	Cu_OF000			[17]
100	Cu_OF100			[17]
200	Cu_OF200			[17]
1	CuP0_300			[5]
2	CuP30_450	175 (4)		[5]
3	CuP60_350	175 (5)		[5]
4	CuP105_450	175 (4)		[5]
6	CuP60_100	175 (4)		[5]
400	Cu-OFP400	215 (5), 250 (3), 300 (4), 350 (2), 400 (2), 450 (1)		[18,19]
500	Cu-OFP500	200 (1), 215 (3), 250 (3), 275 (3), 300 (3), 325 (1), 350 (2)		[18,19]
900	Cu-OFP SSR	20 (2), 75 (4), 125 (4), 175 (4)	Slow strain rate tensile testing; cold worked material	[20]

Table 4
Diffusion coefficients

Species	Type of diffusion	Activation energy Q (kJ/mol)	D_0 (m^2/s)	Reference
Cu self diffusion	Bulk	198.2	1.31×10^{-5}	[21]
Cu self diffusion	Grain boundary	119	1.30×10^{-4}	[23]
Cu self diffusion	Pipe	99	1.31×10^{-5}	[26,27]
P in Cu	Bulk	139	7×10^{-7}	[28]
P in Cu	Grain boundary	83.4	7×10^{-7}	
P in Cu	Pipe	69.5	7×10^{-7}	[26,27]

In Eq. (20), $n(T)$ and $q(T)$ are assumed to be polynomials of T, and $\beta(\sigma)$ a polynomial of σ. For data in the temperature ranges 75–175 °C and 180–250 °C, the fit for Cu-OF is illustrated in Fig. 5. The corresponding fit for Cu-OFP is illustrated in [29]. The constants that have been used in Eq. (20) are given in Table 5.

An effective creep exponent N can be derived from Eq. (20)

$$N = \frac{\partial \log \dot{\varepsilon}_{\mathrm{crmin}}}{\partial \log \sigma} = n(T) + \sigma \frac{\mathrm{d}\beta(\sigma)}{\mathrm{d}\sigma}. \quad (21)$$

The creep exponent N as a function of stress is shown in Fig. 6. The creep exponent increases rapidly with stress and reaches a value of 35 at 170 MPa. Since $n(T)$ is independent of temperature, so is N according to Eq. (21). The creep exponent is even higher for Cu-OFP than for Cu-OF, see Fig. 6. Values from 3 at low stresses to 100 at high stresses are observed.

As can be seen from Fig. 6 there is not a fully continuous transition from the high temperature regime to the low temperature regime. The reason is that there is a dramatic change of creep properties between 175 and 200 °C both

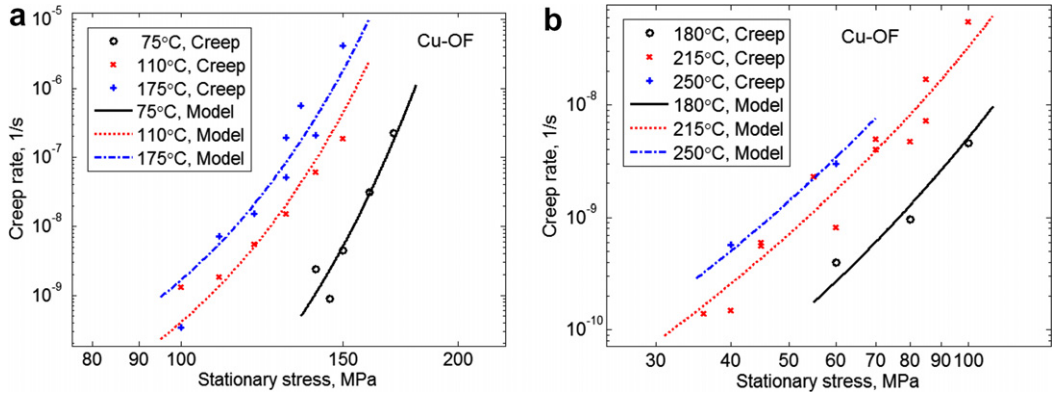

Fig. 5. Creep rate as a function of stress for Cu-OF. (a) Data interval 75–175 °C and (b) data interval 180–250 °C.

Table 5
Constants in Eq. (17)

Material	Temperature range (°C)	A (1/s)	n	β_1 (1/MPa)	β_2 (1/MPa^2)	γ_1 (1/°C)	γ_2 (1/°C^2)
Cu-OF	75–175	6.08×10^{-23}	0	2.00×10^{-2}	4.81×10^{-4}	0.323	-10.56×10^{-4}
Cu-OF	180–250	7.28×10^{-23}	2.90	3.63×10^{-2}	0	0.244	-4.83×10^{-4}
Cu-OFP	20–175	5.40×10^{-23}	0	-9.08×10^{-2}	14.3×10^{-4}	-0.727×10^{-2}	5.46×10^{-4}
Cu-OFP	200–400	3.21×10^{-22}	0	12.6×10^{-2}	1.20×10^{-4}	0.1039	-0.815×10^{-4}

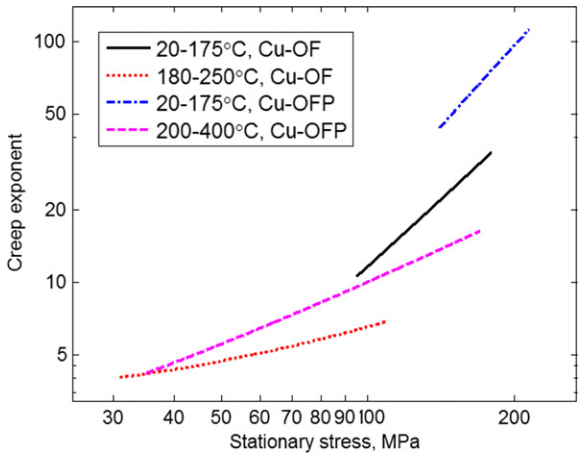

Fig. 6. Creep exponent versus stress for Cu-OFP and Cu-OF in different temperature interval.

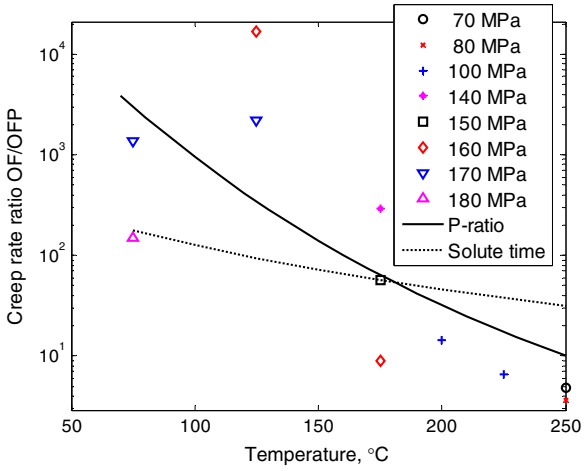

Fig. 7. The ratio in creep rate between Cu-OF and Cu-OFP versus temperature. The experimental points are taken from Figs. 5 and 1 in [29]. The ratio marked solute time is that given in Eq. (9). The curve marked P-ratio is the empirical expression in Eq. (22).

for Cu-OF and Cu-OFP. As a consequence there is a fairly large variation in the observed creep properties in this range. If attempts are made to fit the whole temperature range in one step, the precision in the result is much reduced.

4. Influence of phosphorus

4.1. Creep rate

In Section 2.2, the increased time that it takes for a climbing or gliding dislocation to pass phosphorus atoms in solid solution in comparison to the host atoms was presented. The result is given in Eq. (9). The ratio t_{tot}/t_0 can be considered as an estimate of the ratio between the creep rates of Cu-OF and Cu-OFP. The ratio t_{tot}/t_0 is given as a function of time in Fig. 7.

The comparison with experimental data is made in the following way. For creep rates at different temperatures where there is some overlap in the stress levels for Cu-OF in Fig. 5 and Cu-OFP in Fig. 1 in [29], values are taken from the fitted curves and their ratios are formed. These creep rate ratios are included in Fig. 7. The stress levels are marked in the figure. The model value in Eq. (9) cannot fully represent the temperature dependence of the influence of phosphorus. Eq. (9) is based on an Arrhenius expression for the binding energy between a solute and a dislocation. The model results are of the right order of magnitude, but the temperature dependence is too weak. The binding energy according to Eq. (6) is based on elasticity, and this can only be considered as an estimate in the core region of the dislocation.

For computational purposes in deriving constitutive equations, a fit to the observed values is needed [29]. Due to lack of data a cut-off of the curve is made at 75 °C. The following relation is used:

$$f_P = \frac{\dot{\varepsilon}_{OF}}{\dot{\varepsilon}_{OFP}} = \begin{cases} K_1 \exp(K_2 e^{-k_3 T}) & T > 348\ \text{K} \\ K_0 & T \leqslant 348\ \text{K} \end{cases}, \tag{22}$$

where $K_0 = 3000$, $K_1 = 0.1695$, $K_2 = 55.73$, and $k_3 = 0.005$ 1/°C are constants. In deriving (22) it has also been taken into account that the creep rate ratio is about unity at 400 °C.

4.2. Break stress

With the help of the model in Section 2.4, it is now possible to assess the influence of phosphorus on the creep strength. The creep stress that is required for a given strain rate should be higher for Cu-OFP than for Cu-OF by the amount σ_{break} in Eq. (19). The effect of σ_{break} on the creep rate versus stress curves is illustrated in Fig. 8 for 75–175 °C and in Fig. 9 for 180–250 °C.

The difference between the curves marked Glide and Model is σ_{break} which is the influence of phosphorus on the stationary creep stress at a given creep rate. In the range of experimental data, σ_{break} is up to 40–50 MPa at

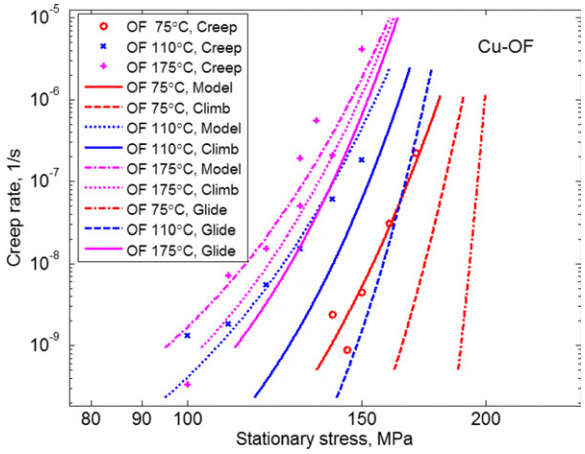

Fig. 8. Creep rate versus stress. Data at 75, 110 and 175 °C are presented forming three groups in the figure. The left hand curve in each group marked Model is together with the creep data the same as in Fig. 5 for Cu-OF. The curves marked Climb (middle curve) and Glide (right hand curve) represent σ_{break} added to the model values for the two deformation mechanisms according to Eq. (19).

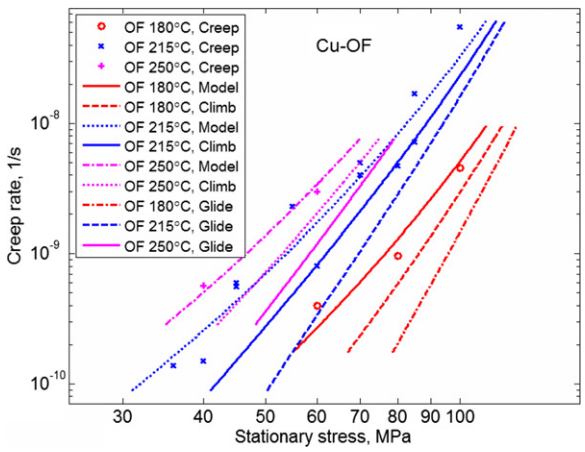

Fig. 9. Same as Fig. 8 for the temperatures 180, 215 and 250 °C.

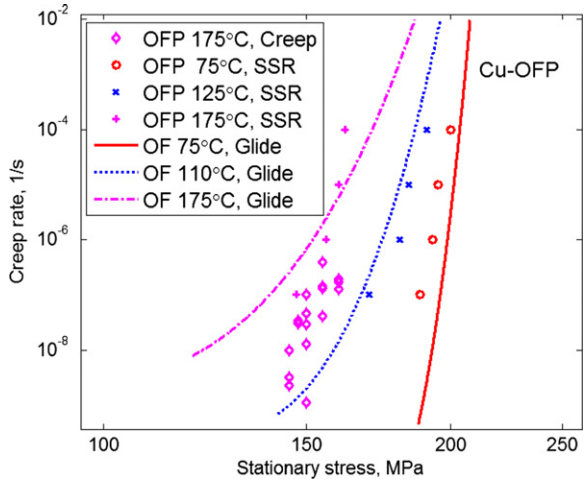

Fig. 10. Creep rate versus stationary stress for Cu-OFP. The prediction is marked Glide that is assumed to be the controlling deformation mechanism. Temperature range 75–175 °C.

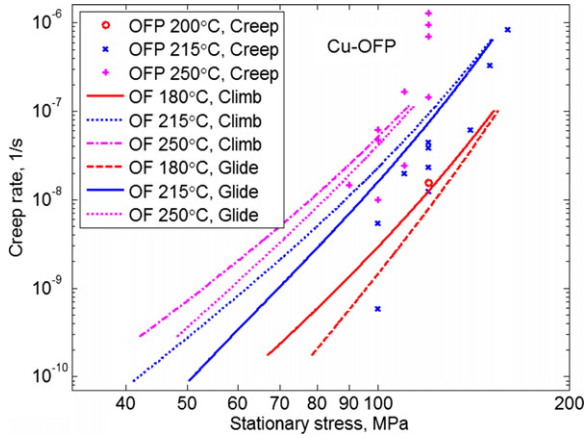

Fig. 11. Same as Fig. 10 for the temperature range 180–250 °C. The curves marked Climb and Glide represent the result when these two mechanisms are controlling.

75 and 110 °C when glide is controlling. At higher temperatures σ_{break} is lower and takes values from 15 to 25 MPa. The values of σ_{break} when climb is controlling are about half of those for glide. That the effect of P is larger for glide than for climb is already evident from the interaction energies in Fig. 2 or from the distribution of solutes in Figs. 3 and 4.

In Figs. 10 and 11 the Climb and Glide curves in Figs. 7 and 8 are compared with experimental results for Cu-OFP.

In the temperature range 75–175 °C, glide can be assumed to be more rapid than climb and the former mechanism is then controlling. Thus, in Fig. 10 only this mechanism is presented. In the range 180–250 °C it is an open question which of the two mechanisms that is dominating and results for both have been included in Fig. 11.

The slopes of the predicted curves in Figs. 10 and 11 agree with the experimental data except at 175 and 250 °C. It is not surprising that these two temperatures cannot be covered since even the parametric fit in Section 3.2 was not able to cope with these temperatures. Concerning the position, the predicted curves can either be to the right of the data (75, 180 and 250 °C) or to the left of the data (110, 175 and 215 °C). This situation can be considered to partially reflect the uncertainty in the creep data.

5. Discussion

The influence of small phosphorus additions on the mechanical properties is remarkable in the sense that the tensile properties are hardly affected whereas the creep properties are strongly changed. The understanding of the low effect on the yield and tensile strength is straightforward. The phosphorus is in solid solution and could possibly give rise to a solid solution hardening effect. In the

present analysis a phosphorus content of 50 wt ppm corresponding to an atomic fraction of 10^{-4} has been assumed. In copper the phosphorus atoms are 16.5% larger than the host atoms and this gives rise to a strain field that increases the strength. In Section 2.1 the solid solution hardening of phosphorus is estimated using Labusch–Nabarro's model. The strength increase is less than 1 MPa, and as expected quite small.

The solid solution could also influence climb which controls the rate of high temperature creep. There are two ways this influence can take place. First, the strain field around the solutes can reduce the climb rate. Second, the solutes must diffuse to or from the dislocation during climb. The first effect gives the correct magnitude of the influence of phosphorus on the creep rate. The second effect is negligible.

Due to the interaction between solutes and the dislocations, a distribution of solutes is formed around each edge dislocation. This is referred to as a Cottrell atmosphere. This situation can be modelled with the help of diffusion equations. According to this solute cloud model there is a strong enhancement of phosphorus atoms close to the dislocations. Due to the form of the interaction energy between a dislocation and a solute as a function of the distance between them, more P-atoms are at the dislocations during glide than during climb. The distribution of solutes gives rise to a drag force. In spite of the large concentrations of P-atoms at the dislocations the drag force is of the order of 1 MPa or less and negligible.

The strong interaction between solutes and dislocations has the consequence that solutes are locked in the core region. In order for a dislocation to move it must break away from the solute cloud. This requires an energy of the order of the maximum binding energy between the solute and the dislocation. To unlock the dislocations, the same energy must be provided by the applied stress. The additional stress required is referred to as the break stress. A model for the break stress is given in Section 2.4. The results show that the predicted break stress is large enough to explain the difference in creep stress between Cu-OF and Cu-OFP. At a given creep rate the break stress is the difference in stationary stress for Cu-OFP and Cu-OF. At least qualitatively the model can describe the differences in creep stress as well as in the stress exponent between the two materials.

6. Conclusions

- The solid solution hardening of 50 wt ppm phosphorus in copper has been estimated with Labusch–Nabarro's model to about 0.7 MPa. This low value is consistent with measured tensile properties.
- The direct solid solution hardening effect on the creep rate has been computed where the additional times for the dislocation to pass a solute and for the solute to diffuse away have been taken into account. The first effect explains the influence of phosphorus on the creep rate although the temperature dependence predicted by model is not accurate. The second effect is negligible.
- Assuming that the P-atoms can freely diffuse around the dislocations, the interaction energy creates a solute cloud, a so-called Cottrell atmosphere. The pronounced increased concentration of P-atoms at the dislocations have been determined. Both the static case with a non-moving dislocation and the dynamic case with a moving dislocation have been analysed. The solute cloud is somewhat larger for a gliding than for a climbing dislocation. An enrichment of up to a factor of 1000 at 75 °C has been found. However, the magnitude of the enrichment is not sufficient to create a significant drag force on the dislocation.
- For a dislocation to move it must break away from the solute cloud. This requires an additional stress, the break stress. This stress has been computed from an energy balance between the work that the applied stress does and the binding energy between a solute and a dislocation. The break stress for unpinning a dislocation from the P-atoms, explains the influence of phosphorus on the creep stress. At a given creep rate the difference in the creep stress between Cu-OFP and of Cu-OF can be described by the model for the break stress. In the experimental range of the creep stresses, the break stress lies in the interval 15–50 MPa. The break stress increases with decreasing temperature and applied stress.

Acknowledgments

The authors wish to thank the Swedish Nuclear Fuel and Waste Management Co. for funding this work.

References

[1] H.L. Burghoff, A.I. Blank, ASTM Proc. 47 (1947) 725.
[2] H.L. Burghoff, A.I. Blank, Trans. AIME 161 (1945) 420.
[3] F.H.H. Kouta, G.A. Webster, in: First International Conference on Current Advances in Mechanical Design and Production, Cairo, 27–27 December 1979, Pergamon, Oxford, 1981, p. 341.
[4] K. Drehfahl, M. Kleinau, W. Steinkamp, Metall. – Int. Z. Tech. Wirt. Heft 5 (1982) 1.
[5] Henrik Andersson, Facredin Seitisleam, Rolf Sandström, Influence of phosphorus and sulphur as well as grain size on creep in pure copper, SKB Report TR-99-39, 1999. <www.skb.se>.
[6] M. Hansen, Constitution of Binary Alloys, McGraw-Hill, 1958.
[7] W.B. Hutchinson, R.K. Ray, Met. Sci. 13 (1979) 125.
[8] R. Sandström, R. Lagneborg, Met. Sci. 9 (1975) 226.
[9] R. Labusch, Acta Metall. 20 (1972) 917.
[10] F.R.N. Nabarro, Philos. Mag. 35 (3) (1977) 613.
[11] H. Sieurin, J. Zander, R. Sandström, Mater. Sci. Eng. A 415 (2006) 66.
[12] H.W. King, J. Mater. Sci. 1 (1966) 79.
[13] ASM Handbook Volume 2. Properties and Selection: Nonferrous Alloys and Special-Purpose Materials, ASM International, 1991.
[14] J.P. Hirth, J. Lothe, Theory of Dislocations, McGraw-Hill, New York, 1968.
[15] J. Friedel, Dislocations, Pergamon, Oxford, 1964.
[16] S. Takeuchi, A.S. Argon, Acta Metall. 24 (1976) 883.
[17] P.J. Henderson, R. Sandström, Mater. Sci. Eng. A246 (1998) 143.

[18] P.J. Henderson, L. Werme, Creep testing of copper for radwaste containers, Euromat 96 "Materials and Nuclear Power", Bournemouth, UK, October 1996.
[19] R. Sandström, J. Test. Eval. 27 (1) (1999) 31.
[20] X.X. Yao, R. Sandström, Study of creep behaviour in P-doped copper with slow strain rate tensile tests, SKB TR-00-09, 2000. <www.skb.se>.
[21] G. Neumann, V. Tölle, C. Tuijn, Physica B: Condens. Matter 271 (1–4) (1999) 21.
[22] D.A. Andersson, S.I. Simak, Phys. Rev. B 70 (2004) 115108.
[23] B. Burton, G.W. Greenwood, Met. Sci. J. 4 (1970) 215.
[24] T. Surholt, Chr. Herzig, Acta Mater. 45 (1997) 3817.
[25] M.R. Sorensen, Y. Mishin, A.F. Voter, Phys. Rev. B (Condens. Matter) 62 (6) (2000) 3658.
[26] Ch. Schwink, A. Nortmann, Mater. Sci. Eng. A 234–236 (1997) 1.
[27] A. Varschavsky, E. Donoso, Mater. Lett. 31 (3–6) (1997) 239.
[28] O. Madelung, (Ed.), Diffusion in Solid Metals and Alloys, Landolt-Börnstein, New Series, Group III/26, Springer-Verlag, Berlin, 1990.
[29] R. Sandström, H.C.M. Andersson, J. Nucl. Mater. 372 (1) (2008) 76.